

LETTER • OPEN ACCESS

Globally prevalent land nitrogen memory amplifies water pollution following drought years

To cite this article: M Lee *et al* 2021 *Environ. Res. Lett.* **16** 014049

View the [article online](#) for updates and enhancements.

ENVIRONMENTAL RESEARCH
LETTERS

LETTER

Globally prevalent land nitrogen memory amplifies water pollution following drought years

OPEN ACCESS

RECEIVED

22 September 2020

REVISED

18 November 2020

ACCEPTED FOR PUBLICATION

8 December 2020

PUBLISHED

11 January 2021

Original content from this work may be used under the terms of the [Creative Commons Attribution 4.0 licence](#).

Any further distribution of this work must maintain attribution to the author(s) and the title of the work, journal citation and DOI.

M Lee^{1,4}, C A Stock², E Shevliakova², S Malyshev² and P C D Milly³ ¹ Program in Atmospheric and Oceanic Sciences, Princeton University, Princeton, NJ, United States of America² NOAA/Geophysical Fluid Dynamics Laboratory, Princeton, NJ, United States of America³ U. S. Geological Survey, Princeton, NJ, United States of America⁴ Author to whom any correspondence should be addressed.E-mail: minjinl@princeton.edu**Keywords:** river nitrogen loads, water pollution, climate variability, nitrogen cycle, watershed model, land model, terrestrial ecosystem modelSupplementary material for this article is available [online](#)

Abstract

Enhanced riverine delivery of terrestrial nitrogen (N) has polluted many freshwater and coastal ecosystems, degrading drinking water and marine resources. An emerging view suggests a contribution of land N memory effects—impacts of antecedent dry conditions on land N accumulation that disproportionately increase subsequent river N loads. To date, however, such effects have only been explored for several relatively small rivers covering a few episodes. Here we introduce an index for quantifying land N memory effects and assess their prevalence using regional observations and global terrestrial-freshwater ecosystem model outputs. Model analyses imply that land N memory effects are globally prevalent but vary widely in strength. Strong effects reflect large soil dissolved inorganic N (DIN) surpluses by the end of dry years. During the subsequent wetter years, the surpluses are augmented by soil net mineralization pulses, which outpace plant uptake and soil denitrification, resulting in disproportionately increased soil leaching and eventual river loads. These mechanisms are most prominent in areas with high hydroclimate variability, warm climates, and ecosystem disturbances. In 48 of the 118 basins analyzed, strong memory effects produce 43% (21%–88%) higher DIN loads following drought years than following average years. Such a marked influence supports close consideration of prevalent land N memory effects in water-pollution management efforts.

1. Introduction

Enhanced riverine delivery of terrestrial nitrogen (N) has impaired the quality of freshwaters for drinking, causing adverse health effects (Ward *et al* 2005), and has contributed to eutrophication of coastal waters (Smith 2003). Coastal impacts are often most acute in the vicinity of river mouths, which funnel loads from diverse upstream sources into restricted and heavily utilized nearshore habitats. Increased river N loads to the coastal ocean have been linked to hypoxic dead zones (Diaz and Rosenberg 2008) and harmful algal blooms (Anderson *et al* 2002) that threaten coastal and marine resources, the economies they support, and public health (Paerl *et al* 1998, Breitburg 2002, UNEP 2006).

Precipitation, resulting river discharge, and their variability have proven to be effective predictors of concurrent river N loads (McIsaac *et al* 2001, Howarth *et al* 2012, Sinha *et al* 2017). A growing number of observational and modeling studies, however, have noted abruptly elevated river N loads or unusual coastal phytoplankton blooms following a drought lasting several months to multiple years (Morecroft *et al* 2000, Acker *et al* 2005, Kaushal *et al* 2008, Lee *et al* 2016, Loecke *et al* 2017). These studies have focused their analyses on relatively small basins (<200 000 km²) and have not explored variations across basins with very different climate and land characteristics.

Determining where, when, and how much such antecedent dry conditions contribute to water

pollution is made difficult by the absence of an analytical framework for quantifying them and the paucity of long-term time series of N monitoring data needed to elucidate river N load responses to climate variability. Understanding the underlying mechanisms is furthermore hindered by the scarcity of direct, basin-scale measurements of concurrent land N storage and its controlling processes (e.g. plant uptake (McFarlane and Yanai 2006), soil denitrification (Groffman et al 2006), net mineralization (Bottomley et al 1994), and leaching).

The capacity of antecedent conditions to influence current ecological processes has been referred to as ‘ecological memory’ (Ogle et al 2015), and consideration of its impacts has improved understanding of tree phenology (Fu et al 2015), ecosystem productivity (Sala et al 2012, Reichmann et al 2013, Ogle et al 2015, Liu et al 2018) and carbon exchanges (Shim et al 2009, Vargas et al 2011, Ogle et al 2015). Aligning with this definition, here we explicitly define ‘land N memory effects’ as impacts of antecedent dry conditions on land N accumulation that disproportionately increase subsequent river N loads. Note that these relatively short-term hydroclimate (dry-wet transition)-driven effects have not been explored for large basins and differ from previously noted long-term legacy effects (Van Meter et al 2018, Vero et al 2018), whereby accumulated N in soils and groundwaters due to past years to decades of land use and agricultural intensification delays the response of river N loads to reductions in anthropogenic N inputs over the next years to decades.

In this study, we introduce a data-driven index for quantifying land N memory effects and assess their global imprint by using available long-term (>30 years), measurement-based data from well-monitored, large (>400 000 km²) basins within the Mississippi River basin (MRB) and outputs from the global terrestrial-freshwater ecosystem model LM3-TAN (Lee et al 2019b). We estimate the degree to which river dissolved inorganic N (DIN) loads from 118 major rivers were amplified by land N memory effects under recent climate during 1981–2010 and classify the basins into nine types according to the strength of memory effects and the amount of DIN loads. Finally, we analyze the model simulations to elucidate the mechanisms underlying global variation in the strength of land N memory effects.

2. Methods

2.1. Quantifying land N memory effects

We decompose the river N load for each year into a linear combination of current- and previous-year river discharge components, with the previous-year discharge providing the dependence on antecedent hydroclimate conditions:

$$\delta L_i = \alpha \delta Q_i - \beta \delta Q_{i-1} + \varepsilon_i \quad (1)$$

where δL_i and δQ_i are, respectively, the annual anomalies of river N load (ktN yr⁻¹) and discharge (m³ s⁻¹) during the year i , δQ_{i-1} is the annual discharge anomaly in the previous year, ε_i is the model error, and α and β are constants. Here, an anomaly is the departure of a variable from its linear trend over time; the mean value of the anomaly over the period of analysis is thus zero. Detrending is used to isolate the effect of hydroclimate variability from the effects of long-term trends in other concurrent factors, such as precipitation, fertilizer applications, and land use. We acknowledge that more sophisticated methods could be used to eliminate such effects, but have not explored them herein. A river basin exhibits a land N memory effect if β is larger than zero, indicating a disproportionately high N load anomaly relative to a discharge anomaly during a year that follows a year having a negative discharge anomaly ($\delta Q_{i-1} < 0$). (The reverse is also true: a prior wet year will suppress the N load anomaly relative to what it would be following an average year.) The mean values of N load and discharge will be denoted by \bar{L} and \bar{Q} .

Under the assumption that the discharge anomaly and model error are neither serially correlated nor cross-correlated, the variance of δL_i is given by

$$\sigma_L^2 = (\alpha^2 + \beta^2) \sigma_Q^2 + \sigma_\varepsilon^2 \quad (2)$$

in which σ_L^2 , σ_Q^2 , and σ_ε^2 are the variances of anomalies of N load and discharge and of model error. It can be seen that land N memory increases the variance of N load. Thus, memory contributes to the occurrence of extreme N loads. Normalizing the N load variance by the part of it that is induced by current-year discharge variance, we have

$$\frac{\sigma_L^2}{\alpha^2 \sigma_Q^2} = (1 + K^2) + \frac{\sigma_\varepsilon^2}{\alpha^2 \sigma_Q^2} \quad (3)$$

in which

$$K = \frac{\beta}{\alpha} \quad (4)$$

K is thus a dimensionless ratio, expressing the dependence of current-year N load on previous-year discharge relative to its dependence on current-year discharge, with high K indicating strong antecedent hydroclimate impacts on N loads relative to the response to contemporaneous hydroclimate. To the extent that the model error is small, land N memory increases the standard deviation of N load by the factor $\sqrt{1 + K^2}$, indicating that the relatively short-term (months to several years) memory (Morecroft et al 2000, Acker et al 2005, Kaushal et al 2008, Lee et al 2016, Loecke et al 2017) does not enhance long-term average N loads, but increase their variability.

From a management perspective, it is critical to quantify how much a previous-year departure of discharge from its mean alters the N load in the current year, relative to what it would have been if β were zero

or if the previous year were a normal discharge year. The relative difference (difference divided by mean) in expected N load can be derived from equation (1) to be $-\beta\delta Q_{i-1}/\bar{L}$. If we adopt the approximation that the intercept of linear load-discharge relation is zero, then $\bar{L} = \alpha\bar{Q}$, and thus the relative difference in N load associated with land N memory is given simply by $-K\delta Q_{i-1}/\bar{Q}$. Therefore, if δQ_{i-1} is expressed as $Z\sigma_Q$, where Z is the number of standard deviations of δQ_{i-1} below the mean, then the relative increase in N load due to land N memory is given by a memory effect index (MEI_Z):

$$MEI_Z = Z \cdot K \cdot CV \quad (5)$$

where CV is the coefficient of variation of discharge anomaly.

K is thus a measure of the intrinsic susceptibility of land to N memory effects, while CV accounts for the hydroclimate variability to which the land is subjected. MEI_Z quantifies the N load enhancement following a year with river discharge Z standard deviations below the mean, relative to the load following an average discharge year. As an example, consider published measurement-based data from the Ohio River at Olmsted, IL (Lee *et al* 2018) (table S1 and figure S1 (available online at stacks.iop.org/ERL/16/014049/mmedia)), for which we find the K equal to 0.25 and CV equal to 0.23. This yields the MEI_2 of 0.12, indicating that the load following a year with river discharge two standard deviations below the mean (hereafter ‘drought’ for our purposes) would be enhanced by 12% relative to the load following an average discharge year. In light of the relevance of large values of MEI_2 to management, we focus on it in our results and discussion.

2.2. Global implementation of the terrestrial-freshwater ecosystem model LM3-TAN

The Geophysical Fluid Dynamics Laboratory (GFDL) Land Model LM3-Terrestrial and Aquatic Nitrogen (TAN) (Lee *et al* 2014, 2019b) simulates coupled water, carbon, and N cycles within a vegetation-soil-river-lake system (Shevliakova *et al* 2009, Gerber *et al* 2010, Milly *et al* 2014). Unlike most empirical watershed models, assuming that N is in steady state and does not accumulate on land, LM3-TAN captures N accumulation within or release from vegetation, soil, and freshwater storage, in response to changes in atmospheric CO₂, climate, anthropogenic N inputs, and land use and land cover (Lee *et al* 2019b). It is thus well suited to simulate land N memory effects. Specifically, LM3-TAN simulates five vegetation functional types based on total biomass and prevailing climate conditions, with their storage updated to account for vegetation growth and allocation, leaf fall and display, and natural and fire-induced mortality. Historically reconstructed scenarios of land-use transitions including the effects of

wood harvesting and shifting cultivation are used to simulate four land-use types: primary lands—lands undisturbed by human activities during land-use reconstruction, secondary lands—abandoned agricultural land or regrowing forest after logging, croplands, and pastures. The model simulates various soil and freshwater microbial processes and associated storage changes, and routing of river flow and N (Lee *et al* 2014, 2019b) for the detailed model descriptions and schematic diagram.

LM3-TAN was globally implemented at 1×1 degree resolution to simulate the past two and half centuries of terrestrial-freshwater N and carbon storage and fluxes to the ocean and atmosphere (Lee *et al* 2019b), considering historical changes in atmospheric CO₂, climate (Sheffield *et al* 2006), anthropogenic N inputs (Green *et al* 2004, Van Drecht *et al* 2009, Bouwman *et al* 2013a), and land use and land cover (Hurtt *et al* 2006). Land N inputs include simulated biological N fixation, synthetic fertilizers (Bouwman *et al* 2013a), and atmospheric deposition (Green *et al* 2004). Land N outputs include river loads to the ocean, emissions to the atmosphere, and net harvest—N in harvested woods, crops, and grasses after subtracting out manure applied to croplands (Bouwman *et al* 2013a) and urban wastewater discharges (Van Drecht *et al* 2009). We note that a recently recognized rock weathering N input (Houlton *et al* 2018) was not added in our model simulations which were evaluated based on traditional terrestrial N budgets without consideration of rock weathering (Galloway *et al* 2004, Ciais *et al* 2013, Bouwman *et al* 2013a). However, we would expect our findings to be insensitive to an addition of this new input, given its small value (15, 11–18 TgN yr⁻¹) (Houlton *et al* 2018) relative to our total N inputs (274, 236–291 TgN yr⁻¹) (Lee *et al* 2019b).

Simulated global, latitudinal, and regional terrestrial-freshwater N and carbon budgets were found to be consistent with published synthesis from 26 different studies, when comparable categorization, definitions, and assumptions were applied (Lee *et al* 2019b). Here we further show that spatial patterns in N use efficiency (which we take as indicative of LM3-TAN capability to simulate plant uptake) and soil denitrification are consistent with published estimates (Bouwman *et al* 2013b, Lassaletta *et al* 2016) (table S2 and figure S2).

In this study, we used the global LM3-TAN outputs (Lee *et al* 2019b) to explore land N memory effects and the underlying mechanisms. For comparison of LM3-TAN-based memory effects with measurement-based estimates (figure 1), ~35 years (~1976–2010) of annual outputs were used to match the measurement periods (table S1). For global analyses (figures 2–4), 30 years (1981–2010) of annual outputs were used. Among 159 major rivers (of which basin areas and log10 of discharges are, respectively, larger than 100 000 km² and 2.2), we excluded,

for the memory effect analyses, 41 basins exhibiting insignificant α in equation (1) at the 0.01 level (lightest grey shade in figure 2(a)). This filters out rivers where interannual variability of N loads is not significantly related to contemporaneous hydroclimate variability due to the predominance of other factors (e.g. abrupt changes in land use and anthropogenic N inputs) that fall outside the scope of our analysis and are not effectively removed by detrending. The MEI_Z associated with hydroclimate variability (i.e. equation (5)) cannot be reliably defined in cases where α cannot be statistically distinguished from 0 (β/α is undefined at $\alpha = 0$). Application of this filter left 118 of 159 rivers for which MEI_Z could be reliably calculated.

2.3. Baseline and sensitivity simulations

Storage, input and output fluxes of N in many terrestrial and freshwater ecosystems remain uncertain due to sparse measurements (Galloway *et al* 2004, 2008, Gruber and Galloway 2008). To quantify uncertainties, a baseline simulation was defined, and sensitivity simulations were repeated with various forcings (Lee *et al* 2019b). The baseline simulation simulated global biological N fixation near the center of published ranges (128, 112–139 TgN yr⁻¹) (Galloway *et al* 2004, Green *et al* 2004), used fertilizer inputs from Bouwman *et al* (2013a), and a land use and land cover change scenario including the effects of wood harvesting and shifting cultivation (Hurt *et al* 2006).

The sensitivity simulations were forced with biological N fixation settings producing simulations that spanned the upper (116 TgN yr⁻¹) and lower (145 TgN yr⁻¹) bounds of the published ranges (Galloway *et al* 2004, Green *et al* 2004), different fertilizer inputs from Lu and Tian (Lu and Tian 2017), a different land use and land cover change scenario without shifting cultivation (Hurt *et al* 2006), and different fractions to divide anthropogenic N inputs into three N species of organic, ammonium, and nitrate plus nitrite N (USEPA 2010, Lamarque *et al* 2013). In recognition of the uncertainty surrounding the degree of CO₂ fertilization effects on terrestrial C sinks (Gregory *et al* 2009, Huntzinger 2017), robustness of the results to a scenario with no CO₂ fertilization was also considered. See Lee *et al* (2019b) for a detailed description of model forcing and simulations.

3. Results

3.1. Land N memory effect variation across the MRB

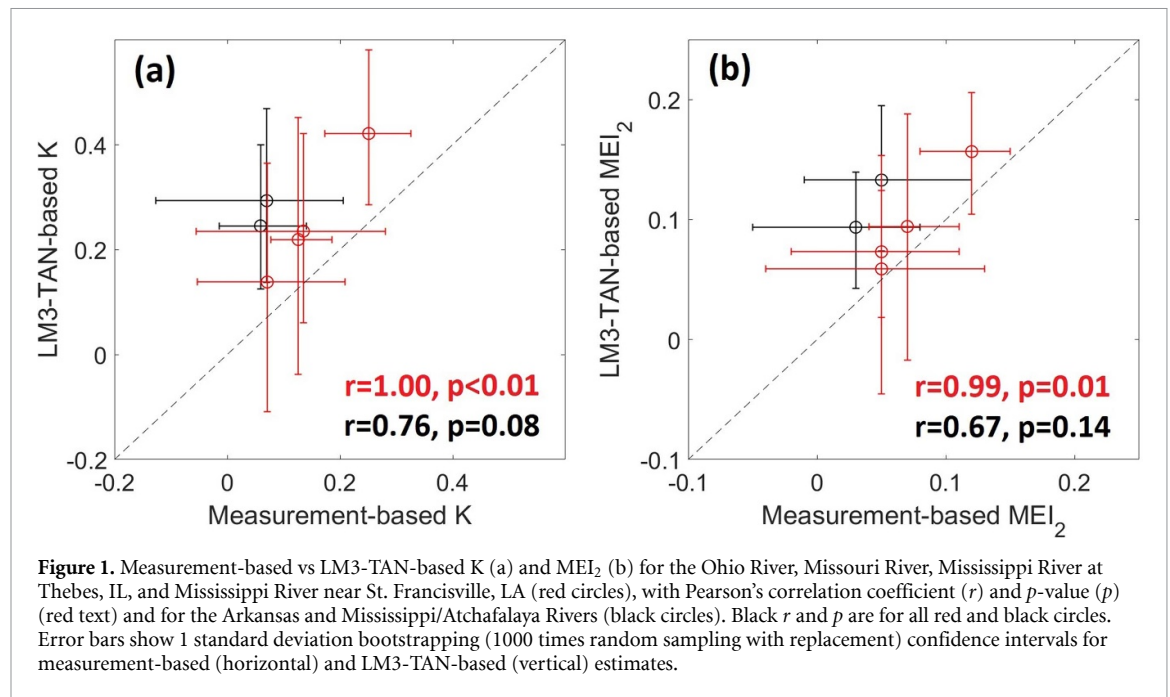
An analysis of K and MEI_Z calculated by using long-term (>30 years) observed annual river discharges and published, measurement-based estimates of annual inorganic N loads from the large (>400 000 km²), well-monitored river basins inside

the MRB (Aulenbach *et al* 2007, Lee *et al* 2018) (See table S1 and figure S1 for a data description and map of the basins) reveals that land N memory effects vary across the basin (figure 1). In headwaters of the MRB, a significant land N memory affects Ohio River loads ($MEI_Z = 0.12$, 0.08–0.15), while the effect is insignificant for Missouri River loads ($MEI_Z = 0.05$, –0.04–0.13). The aggregation of these basins at the Mississippi River at Thebes, IL yields an intermediate, marginally significant effect ($MEI_Z = 0.07$, 0.04–0.11) that becomes weakened through the main stem Mississippi River ($MEI_Z = 0.05$, –0.02–0.11) after integrating a signal without a memory effect from the Arkansas River measured at Murray Dam, AR ($MEI_Z = 0.05$, –0.01–0.12). A memory effect for loads from the whole MRB (including the portion of its discharge that flows through the Atchafalaya River) becomes insignificant ($MEI_Z = 0.03$, –0.05–0.08).

Despite the limited resolution of subbasins within the MRB in the globally implemented LM3-TAN and the limited strength of measurement-based memory effects (i.e. $MEI_Z < 0.2$), LM3-TAN captures variation in the strength throughout the main stem Mississippi River (red circles in figure 1). However, unlike the measurement-based estimates, LM3-TAN shows significant memory effects for Arkansas and Mississippi/Atchafalaya River loads (black circles). The global implementation of LM3-TAN poorly resolves the Arkansas and Atchafalaya River Basins (figure S1) and does not account for complex hydraulic controls in both rivers that could subvert natural memory effects. While long-term data sets for validating simulated land N memory effects are admittedly limited and themselves subject to uncertainty (Lee *et al* 2019a; see section 4), the consistency between LM3-TAN-based and measurement-based memory effect estimates along the main stem Mississippi River supports further analysis of the potential global extent of land N memory effects and the mechanisms that underlie them. We note, however, that LM3-TAN estimates likely represent an upper bound on the memory effect, particularly for rivers under strong hydraulic controls.

3.2. Globally prevalent land N memory effects

LM3-TAN-based estimates of MEI_Z for the period 1981–2010 suggest that land N memory effects are globally prevalent yet vary widely in strength (figure 2(a)). Of the 118 major river basins, 85 basins (accounting for 67% by area) exhibit significant memory effects at the 0.1 level ($MEI_Z > 0$) and 48 basins (accounting for 32% by area) enhanced DIN loads by over 20% following drought years relative to those following average years ($MEI_Z > 0.2$). These results are robust to different partitioning assumptions for anthropogenic N inputs into different N species (USEPA 2010, Lamarque *et al* 2013), biological N fixation parameters spanning the upper and lower bounds of published ranges (Galloway *et al* 2004,



Green *et al* 2004), scenarios of land use and land cover change (Hurt *et al* 2006), levels of CO_2 fertilization, and fertilizer input datasets (Bouwman *et al* 2013a, Lu and Tian 2017) (figure S3).

We classify the 118 basins into 9 types according to the strength of memory effects (as measured by MEI_2) and the magnitude of long-term (1981–2010) mean river DIN loads (figure 2(a)). For example, basins (B) characterized by strong (S, $MEI_2 > 0.2$) memory effects and high (H, $DIN > 100 \text{ ktN yr}^{-1}$) DIN loads are designated as ' $B_{S,H}$ '. This basin type likely poses the highest pollution potential following drought years; that is, strong memory effects further amplify already high DIN loads (generally due to high long-term mean anthropogenic N inputs or large basin area). The potential spatiotemporal extent of pollution declines for moderate (M, $20 \text{ ktN yr}^{-1} < DIN \leq 100 \text{ ktN yr}^{-1}$) and low (L, $DIN \leq 20 \text{ ktN yr}^{-1}$) load basins with strong memory effects ($B_{S,M}$ and $B_{S,L}$), though the potential for localized acute impacts remains.

Strong and weak (W, $0 < MEI_2 \leq 0.2$) memory effect basins, respectively, produce 43% (21%–88%) and 13% (3%–20%) higher DIN loads after drought years than after average years (figure 2(b)). In basins with no (N, $MEI_2 \leq 0$) memory effects, DIN loads following drought years are essentially no greater than those following any other years. It is noteworthy that many $B_{S,H}$, $B_{S,M}$, and $B_{W,H}$ type basins posing high pollution potentials (e.g. Mississippi, Vistula, Rhine, Elbe, Yellow) are located in regions with documented severe coastal water pollution associated with river N loads (e.g. Gulf of Mexico (Turner *et al* 2008), Baltic (Eriksson *et al* 2007, Conley 2012), Wadden (Van Beusekom 2018), North (Van Beusekom 2018), and Yellow (Liu *et al* 2013) Seas).

3.3. Mechanisms underlying land N memory effects

To understand the mechanisms underlying land N memory effects, we trace land N memory from its origins within the river basins to its manifestation at the river mouths. For each basin, the mean of DIN storage or flux anomalies for the ten driest years during the period 1981–2009 (red box plots, figure 3) and for the following ten wetter years (blue box plots) was calculated. Figures 3(a)–(d), respectively, show composites of the means for high load systems with strong and no memory effects ($B_{S,H}$ and $B_{N,H}$).

In strong-memory/high-load $B_{S,H}$ basins, dry years begin, on average, with soil DIN storage near historical means (figure 3(a)). Reductions in plant uptake, soil denitrification and leaching, however, all contribute to considerable soil DIN surpluses by the end of the dry years (moving from left to right in figure 3(a)). During the subsequent wetter years, the considerable surpluses are further augmented by soil net mineralization pulses (Xiang *et al* 2008, Borken and Matzner 2009). Plant uptake and soil denitrification are also enhanced, but not by enough to prevent significantly elevated soil leaching to rivers. Once in the rivers, the elevated leaching is eroded by increased freshwater denitrification, but buoyed by enhanced mineralization of organic N (figure 3(b)). This results in positive DIN load anomalies at the river mouths.

In no-memory/high-load $B_{N,H}$ basins, negative anomalies of plant uptake, soil denitrification and leaching during the dry years and resulting soil surpluses are much smaller than those exhibited by the $B_{S,H}$ basins (figure 3(c)). Furthermore, during the subsequent wetter years, nearly neutral soil net mineralization does not supplement the smaller surpluses, which are effectively consumed by plant

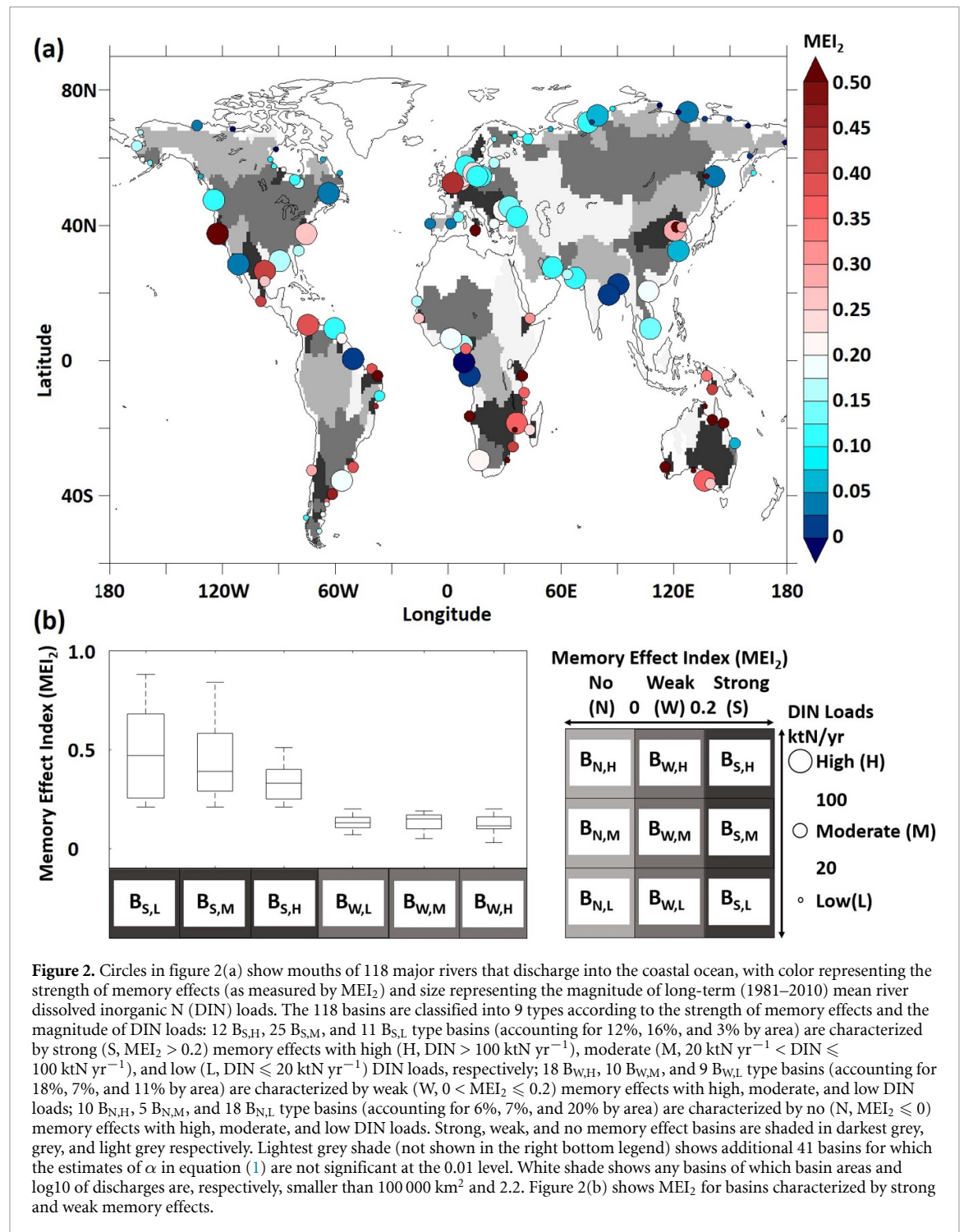
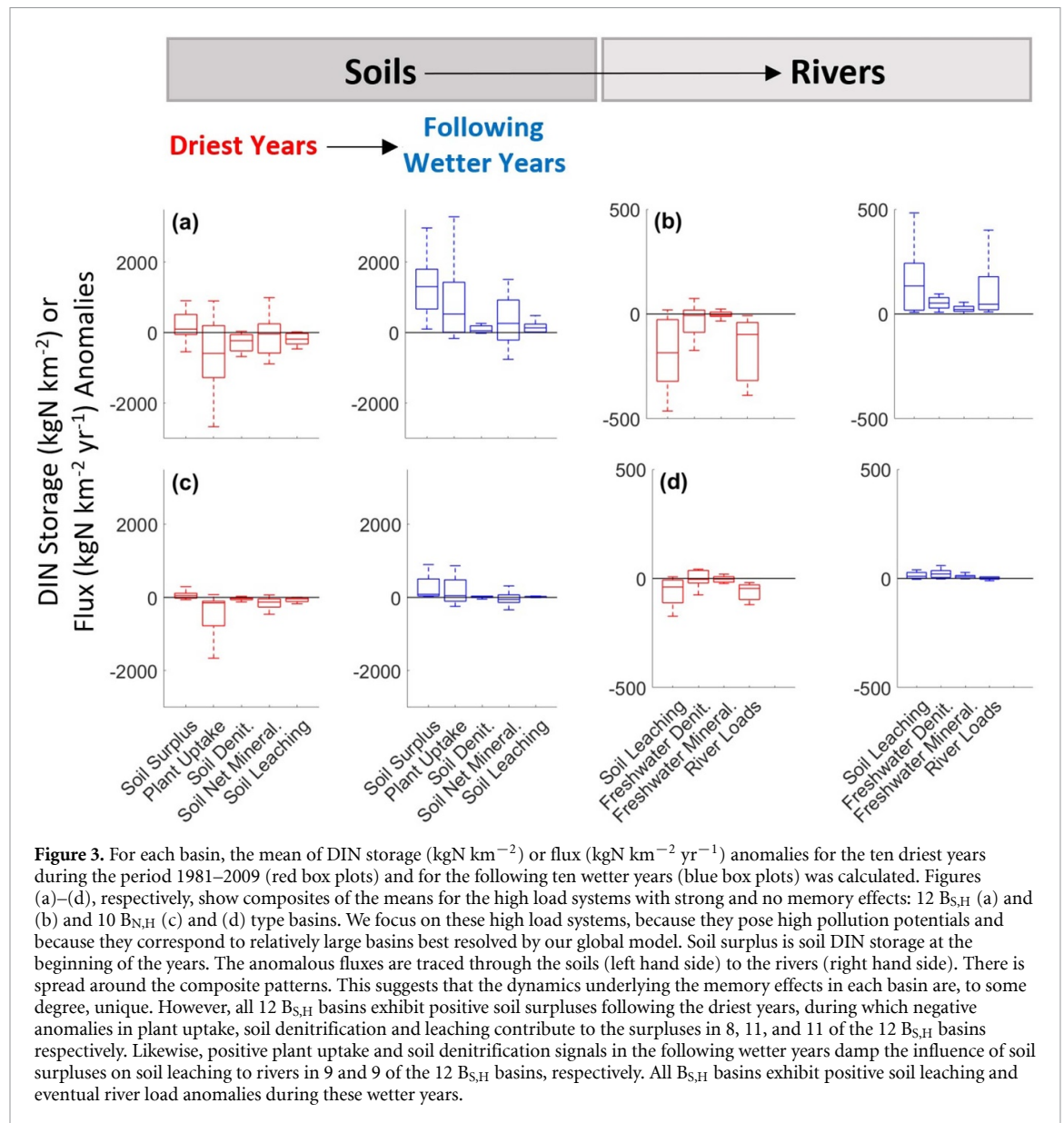


Figure 2. Circles in figure 2(a) show mouths of 118 major rivers that discharge into the coastal ocean, with color representing the strength of memory effects (as measured by MEI_2) and size representing the magnitude of long-term (1981–2010) mean river dissolved inorganic N (DIN) loads. The 118 basins are classified into 9 types according to the strength of memory effects and the magnitude of DIN loads: 12 $B_{S,H}$, 25 $B_{S,M}$, and 11 $B_{S,L}$ type basins (accounting for 12%, 16%, and 3% by area) are characterized by strong (S, $MEI_2 > 0.2$) memory effects with high (H, $DIN > 100 \text{ ktN yr}^{-1}$), moderate (M, $20 \text{ ktN yr}^{-1} < DIN \leq 100 \text{ ktN yr}^{-1}$), and low (L, $DIN \leq 20 \text{ ktN yr}^{-1}$) DIN loads, respectively; 18 $B_{W,H}$, 10 $B_{W,M}$, and 9 $B_{W,L}$ type basins (accounting for 18%, 7%, and 11% by area) are characterized by weak (W, $0 < MEI_2 \leq 0.2$) memory effects with high, moderate, and low DIN loads; 10 $B_{N,H}$, 5 $B_{N,M}$, and 18 $B_{N,L}$ type basins (accounting for 6%, 7%, and 20% by area) are characterized by no (N, $MEI_2 \leq 0$) memory effects with high, moderate, and low DIN loads. Strong, weak, and no memory effect basins are shaded in darkest grey, grey, and light grey respectively. Lightest grey shade (not shown in the right bottom legend) shows additional 41 basins for which the estimates of α in equation (1) are not significant at the 0.01 level. White shade shows any basins of which basin areas and log10 of discharges are, respectively, smaller than $100\,000 \text{ km}^2$ and 2.2. Figure 2(b) shows MEI_2 for basins characterized by strong and weak memory effects.

uptake, leaving soil leaching, and eventual river loads, near average levels (figure 3(d)).

While the large spread in the $B_{S,H}$ and $B_{N,H}$ composites in figure 3 suggests considerable basin-specific variations, their contrast suggests a leading role of relatively low plant uptake and high soil net mineralization pulses following dry years in promoting land N memory signals to rivers. We next investigate which observable, basin-scale climate and land characteristics, interacting with the ecological and biogeochemical mechanisms described above, determine the strength of land N memory effects.

According to equation (5), the strength of land N memory effects (MEI_2) depends on a combination of hydroclimate variability, captured by CV, and additional factors determining K . We use a stepwise linear regression to identify possible controls on MEI_2 across the 118 basins (shown in figure 2(a)) by climate and land characteristics—climate mean and variability (precipitation, soil moisture, runoff, river discharge, air temperature, and their standard deviations), anthropogenic N inputs, basin area, and land use type. The use of stepwise regression partially obviates the problem of cross-correlation among the

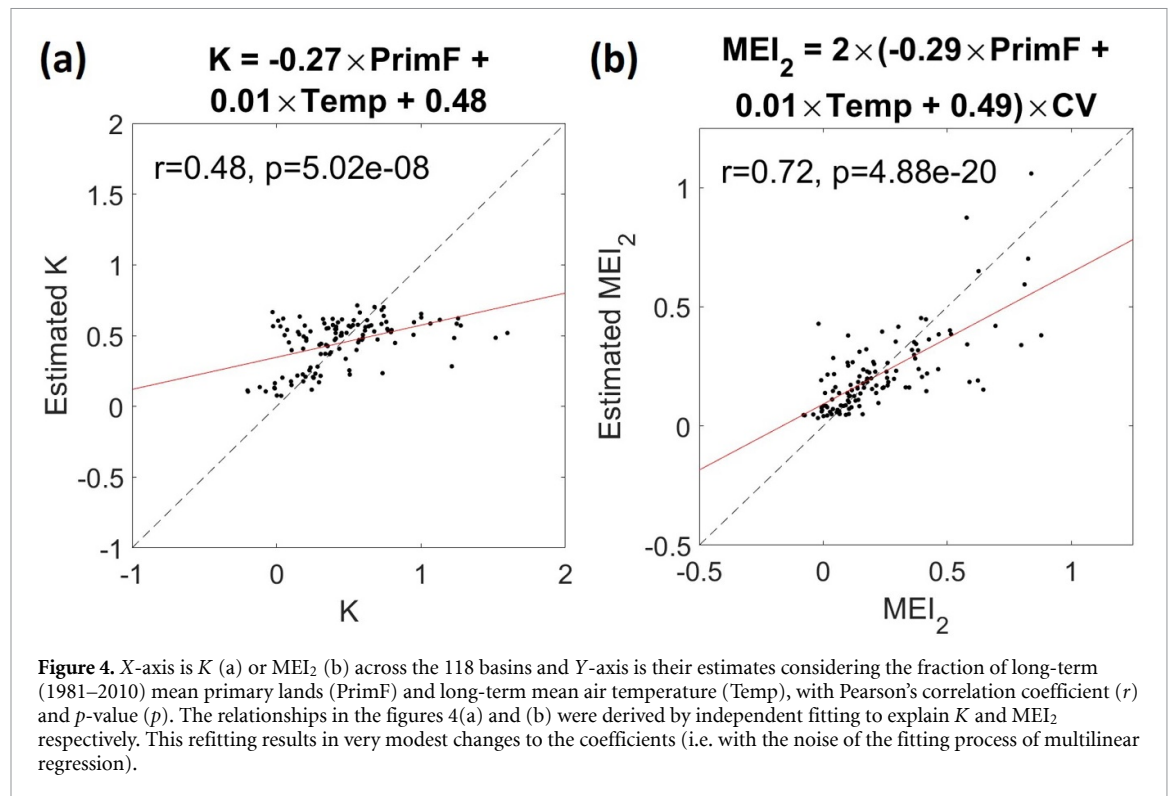


predictor variables. We find that the fraction of previously undisturbed, primary lands (figure S4) and air temperature emerge clearly as two primary factors governing the K variation ($r = 0.48$, figure 4(a)). Combining these predictors with the direct dependence on CV, we obtain the overall correlation with LM3-TAN-derived MEI_2 of 0.72 (figure 4(b)). Thus, high hydroclimate variability is a key driver of variation in the memory effect strength, and anthropogenic land disturbances and warm climates can amplify hydroclimate effects. We show that this result is robust to the exclusion of 28 and 65 basins exhibiting insignificant α in equation (1) at the 0.5 and 0.001 level, respectively (figure S5).

4. Discussion and conclusion

While there are very limited observations of contemporaneous N processes to constrain the simulated global land N memory effect patterns,

our combined analyses of regional observations and global LM3-TAN simulations provide a unique insight into land N memory effects and the underlying mechanisms. Strong memory effects reflect relatively low plant N uptake following dry years (figure 3), which aligns with long-term data analysis and experimentation showing legacies of dry years leading to below-average primary production even upon returning to average precipitation years (Sala *et al* 2012, Reichmann *et al* 2013). Attributing such low plant uptake to a large fraction of disturbed lands (figure 4) is further supported by pronounced dry-year legacy effects on primary production found in grasslands (Sala *et al* 2012, Reichmann *et al* 2013). On the other hand, relatively high soil net mineralization pulses following dry years in the strong memory effect basins are attributed to low hydrophobicity of grassland and cropland soils (Borken and Matzner 2009) and to warm climates with fast mineralization rates (Haney *et al* 2004) (figures 3



and 4). These results are consistent with previously observed memory effects exhibited by basins including large agricultural or urban areas (Morecroft *et al* 2000, Acker *et al* 2005, Kaushal *et al* 2008, Lee *et al* 2016, Loecke *et al* 2017), as well as the measurement-based memory effect contrasts between the Ohio and Missouri Rivers shown in figure 1. The former basin, influenced by a larger fraction of disturbed lands and warmer climates, exhibits stronger memory effects.

Important factors that are not resolved in LM3-TAN include the potential role of hydraulic controls (e.g. dams, reservoirs, and irrigation) in shaping land N memory effects. Retaining waters in dams and reservoirs would presumably act as a buffer, causing river loads to be less sensitive to natural hydroclimate variability. The absence of these controls in the model thus suggests that the model results present an upper bound of memory effects, particularly for basins under strong hydraulic controls. Irrigation would presumably limit soil N buildup during droughts, and thus also weaken memory effects. However, we would not expect that this has significantly impacted our primary findings given that irrigated land (Siebert *et al* 2015) covers only 2% of global land area and 6% of global agricultural land area. We also note that this limitation does not prevent LM3-TAN simulations of river discharge, dissolved inorganic and organic N loads and concentrations from showing robust agreements with measurement-based estimates across 47 globally distributed rivers ($r = 0.74\text{--}0.91$) (Lee *et al* 2019). Moreover, the agreement of LM3-TAN simulation of DIN loads with measurement-based estimates

($r = 0.82$) is comparable with that of a land surface and river transport model that includes irrigation (Liu *et al* 2019).

In addition, our theoretical framework for the land N memory effect index rests on the capacity to estimate the ratio of the previous-year hydroclimate impacts on current-year river N loads, relative to the current-year hydroclimate impacts (i.e. $K = \beta/\alpha$ in equation (5)). The scope of our index is thus limited to those basins, exhibiting significant current-year discharge-N load relationships ($\alpha \neq 0$) against which the dependence to the previous-year discharge can be judged (β/α is undefined at $\alpha = 0$). Other factors (e.g. abrupt changes in land use and anthropogenic N inputs) can modulate the response of each basin to hydroclimate variability, but our approach cannot capture memory effects in systems with very weak discharge-N load relationships, or those that have been significantly and non-linearly interrupted by factors that cannot be captured with the simple detrending applied herein. Further consideration of memory effects in such basins requires closer inspection of basin-specific trajectories and dynamics that we leave to future basin-specific studies.

Finally, our results highlight the relative paucity of long time series of measurement-based river N load estimates for validating model dynamics (figure 1). In addition, available measurement-based estimates of annual N loads are themselves fraught with methodological details related to sampling and analytical procedures, as well as statistical methods that use relatively frequent (e.g. daily) discharge observations to calculate continuous N concentrations, in the absence

of frequent N samples (Lee *et al* 2019a). In fact, some statistical methods appear to reduce the strength of memory effects (table S3). This might explain, in part, higher LM3-TAN-based K and MEI₂ than measurement-based ones shown in figure 1. Thus, a commitment to fostering long-term, frequent N sampling and further scrutiny of the impacts of using different N load estimation methods on memory effect analyses are both essential for strengthening the observational foundations of this globally relevant phenomena.

River basins are projected to experience dramatic shifts in hydroclimate variability, warming, land use (IPCC 2019)—the primary governing factors of emergent land N memory effects in our global model simulations. Projected increases in severe droughts, precipitation extremes, and temperature due to climate change (Coumou and Rahmstorf 2012, Dai 2013, IPCC 2019) may accentuate memory effects to amplify river N load extremes in many regions. Furthermore, continuous development in tropical regions (McIntyre *et al* 2009, Hurtt *et al* 2011, IPCC 2019) may convert no-memory/high-load basins like the Amazon to be more sensitive to drying–rewetting stress, and thus exacerbate existing severe water N pollution (Wang *et al* 2019). We thus conclude by stressing the necessity to carefully consider hydroclimate-associated memory effects for future water-pollution policies and mitigation strategies.

Data availability

Reported river discharge and empirical estimates of river inorganic (NO₂+NO₃+NH₃) N loads at the Mississippi River near St. Franciswill, LA, and Atchafalaya River at Melville, LA, are available at (https://toxics.usgs.gov/hypoxia/mississippi/flux_est/delivery/Gulf-Monthly-2016.xlsx) (Aulenbach *et al* 2007); last accessed 22 September 2020. The other four data of discharges and N loads within MRB are available at (www.sciencebase.gov/catalog/item/5af49c2ae4b0da30c1b44e2b) (Lee *et al* 2018); last accessed 22 September 2020.


The data that support the findings of this study are available upon reasonable request from the authors.

Acknowledgments

We thank John Dunne from NOAA/Geophysical Fluid Dynamic Laboratory for incisive comments on the manuscript. This report was prepared by Minjin Lee under award NA18OAR4320123 from the National Oceanic and Atmospheric Administration, U.S. Department of Commerce. The statements, findings, conclusions, and recommendations are those of the authors and do not necessarily reflect the views

of the National Oceanic and Atmospheric Administration, or the U.S. Department of Commerce. The authors declare no competing interests.

ORCID iDs

S Malyshev  <https://orcid.org/0000-0001-6259-1043>

P C D Milly  <https://orcid.org/0000-0003-4389-3139>

References

- Acker J G, Harding L W, Leptoukh G, Zhu T and Shen S 2005 Remotely-sensed chl a at the Chesapeake Bay mouth is correlated with annual freshwater flow to Chesapeake Bay *Geophys. Res. Lett.* **32** L05601
- Anderson D M, Glibert P M and Burkholder J M 2002 Harmful algal blooms and eutrophication: nutrient sources, composition, and consequences *Estuaries* **25** 704–26
- Aulenbach B T, Buxton H T, Battaglin W T and Coupe R H 2007 Streamflow and nutrient fluxes of the Mississippi-Atchafalaya River Basin and subbasins for the period of record through 2005 U.S. Geological Survey Open-File Report 2007-1080
- Borken W and Matzner E 2009 Reappraisal of drying and wetting effects on C and N mineralization and fluxes in soils *Glob. Change Biol.* **15** 808–24
- Bottomley P J, Weaver R W and Angle J S 1994 *Methods of Soil Analysis: Part 2—Microbiological and Biochemical Properties* (Madison: Soil Science Society of America, Inc.) ch 42
- Bouwman A F, Beusen A H W, Griffioen J, Van Groenigen J W, Hefting M M, Oenema O, Van Puijenbroek P J T M, Seitzinger S, Slomp C P and Stehfest E 2013b Global trends and uncertainties in terrestrial denitrification and N₂O emissions *Phil. Trans. R. Soc. B* **368** 20130112
- Bouwman L, Goldewijk K K, Van Der Hoek K W, Beusen A H W, Van Vuuren D P, Willems J, Rufino M C and Stehfest E 2013a Exploring global changes in nitrogen and phosphorus cycles in agriculture induced by livestock production over the 1900–2050 period *Proc. Natl Acad. Sci. USA* **110** 20882–7
- Breitburg D 2002 Effects of hypoxia, and the balance between hypoxia and enrichment, on coastal fishes and fisheries *Estuaries* **25** 767–81
- Ciais P C *et al* 2013 Carbon and other biogeochemical cycles *Climate Change 2013: The Physical Science Basis*, ed T F Stocker *et al* (Cambridge: Cambridge University Press) pp 465–570
- Conley D J 2012 Save the Baltic Sea *Nature* **486** 463–4
- Coumou D and Rahmstorf S 2012 A decade of weather extremes *Nat. Clim. Change* **2** 491–6
- Dai A 2013 Increasing drought under global warming in observations and models *Nat. Clim. Change* **3** 52–58
- Diaz R J and Rosenberg R 2008 Spreading dead zones and consequences for marine ecosystems *Science* **321** 926–9
- Eriksson H, Pastuszak M, Lofgren S, Morth C and Humborg C 2007 Nitrogen budgets of the Polish agriculture 1960–2000: implications for riverine nitrogen loads to the Baltic Sea from transitional countries *Biogeochemistry* **85** 153–68
- Fu Y H *et al* 2015 Declining globalwarming effects on the phenology of spring leaf unfolding *Nature* **526** 104–8
- Galloway J N *et al* 2004 Nitrogen cycle: past, present and future *Biogeochemistry* **70** 153–226
- Galloway J N, Townsend A R, Erismann J W, Bekunda M, Cai Z, Freney J R, Martinelli L A, Seitzinger S P and Sutton M A 2008 Transformation of the nitrogen cycle: recent trends, questions, and potential solutions *Science* **320** 889–92
- Gerber S, Hedin L O, Oppenheimer M, Pacala S W and Shevliakova E 2010 Nitrogen cycling and feedbacks in a

- global dynamic land model *Glob. Biogeochem. Cycles* **24** GB1001
- Green P A *et al* 2004 Pre-industrial and contemporary fluxes of nitrogen through rivers: a global assessment based on typology *Biogeochemistry* **68** 71–105
- Gregory J M, Jones C D, Cadule P and Friedlingstein P 2009 Quantifying carbon cycle feedbacks *J. Clim.* **22** 5232–50
- Groffman P M *et al* 2006 Methods for measuring denitrification: diverse approaches to a difficult problem *Ecol. Appl.* **16** 2091–122
- Gruber N and Galloway J N 2008 An Earth-system perspective of the global nitrogen cycle *Nature* **451** 293–6
- Haney R L, Franzluebbers A J, Porter E B, Hons F M and Zuberer D A 2004 Soil carbon and nitrogen mineralization: influence of drying temperature *Soil Sci. Soc. Am. J.* **68** 489–92
- Houlton B Z, Morford S L and Dahlgren R A 2018 Convergent evidence for widespread rock nitrogen sources in Earth's surface environment *Science* **360** 58–62
- Howarth R, Swaney D, Billen G, Garnier J, Hong B, Humborg C, Johnes P, Mörtz C-M and Marino R 2012 Nitrogen fluxes from the landscape are controlled by net anthropogenic nitrogen inputs and by climate *Front. Ecol. Environ.* **10** 37–43
- Huntzinger D N 2017 Uncertainty in the response of terrestrial carbon sink to environmental drivers undermines carbon-climate feedback predictions *Sci. Rep.* **7** 4765
- Hurt G C *et al* 2006 The underpinnings of land-use history: three centuries of global gridded land-use transitions, wood-harvest activity, and resulting secondary lands *Glob. Change Biol.* **12** 1208–29
- Hurt G C *et al* 2011 Harmonization of land-use scenarios for the period 1500–2100: 600 years of global gridded annual land-use transitions, wood harvest, and resulting secondary lands *Clim. Change* **109** 117–61
- IPCC 2019 *Climate Change and Land: An IPCC Special Report on Climate Change, Desertification, Land Degradation, Sustainable Land Management, Food Security, and Greenhouse Gas Fluxes in Terrestrial Ecosystems*, ed P R Shukla *et al* accepted (www.ipcc.ch/srccl/)
- Kaushal S, Groffman P M, Band L E, Shields C A, Morgan R P, Palmer M A, Belt K T, Swan C M, Findlay S E G and Fisher G T 2008 Interaction between urbanization and climate variability amplifies watershed nitrate export in Maryland *Environ. Sci. Technol.* **42** 5872–8
- Lamarque J F *et al* 2013 Multi-model mean nitrogen and sulfur deposition from the atmospheric chemistry and climate model intercomparison project (ACCMIP): evaluation of historical and projected future changes *Atmos. Chem. Phys.* **13** 7997–8018
- Lassaletta L, Billen G, Garnier J, Bouwman L, Velazquez E, Mueller N D and Gerber J S 2016 Nitrogen use in the global food system: past trends and future trajectories of agronomic performance, pollution, trade, and dietary demand *Environ. Res. Lett.* **11** 095007
- Lee C J, Hirsch R M and Crawford C G 2019a An evaluation of methods for computing annual water-quality loads: U.S. Geological Survey Scientific Investigations Report 2019–5084
- Lee C J, Norma J E and Reutter D C 2018 Nutrient and pesticide data collected from the USGS National Water Quality Network and previous networks, 1963–2017 U.S. Geological Survey data release (<https://doi.org/10.5066/P9TMSQFE>)
- Lee M, Malyshev S, Shevliakova E, Milly P C D and Jaffé P R 2014 Capturing interactions between nitrogen and hydrological cycles under historical climate and land use: Susquehanna watershed analysis with the GFDL Land Model LM3-TAN *Biogeosciences* **11** 5809–26
- Lee M, Shevliakova E, Malyshev S, Milly P C D and Jaffé P R 2016 Climate variability and extremes, interacting with nitrogen storage, amplify eutrophication risk *Geophys. Res. Lett.* **43** 7520–8
- Lee M, Shevliakova E, Stock C A, Malyshev S and Milly P C D 2019b Prominence of the tropics in the recent rise of global nitrogen pollution *Nat. Commun.* **10** 1437
- Liu D, Keesing J K, He P, Wang Z, Shi Y and Wang Y 2013 The world's largest macroalgal bloom in the Yellow Sea, China: formation and implications *Estuar. Coast. Shelf Sci.* **129** 2–10
- Liu L, Zhang Y, Wu S, Li S and Qin D 2018 Water memory effects and their impacts on global vegetation productivity and resilience *Sci. Rep.* **8** 2962
- Liu S *et al* 2019 Effects of anthropogenic nitrogen discharge on dissolved inorganic nitrogen transport in global rivers *Glob. Change Biol.* **25** 1493–513
- Loecke T D, Burgin A J, Riveros-Iregui D A, Ward A S, Thomas S A, Davis C A and Clair M A S 2017 Weather whiplash in agricultural regions drives deterioration of water quality *Biogeochemistry* **133** 7–15
- Lu C and Tian H 2017 Global nitrogen and phosphorus fertilizer use for agriculture production in the past half century: shifted hot spots and nutrient imbalance *Earth Syst. Sci. Data* **9** 181–92
- McFarlane K J and Yanai R D 2006 Measuring nitrogen and phosphorus uptake by intact roots of mature *Acer saccharum* Marsh., *Pinus resinosa* Ait., and *Picea abies* (L.) Karst *Plant Soil* **279** 163–72
- McIntyre B D, Herren H R, Wakhungu J and Watson R T 2009 *Agriculture at a Crossroads the Synthesis Report of the International Assessment of Agricultural Knowledge, Science and Technology for Development (IAASTD)* (Washington DC: Island Press)
- McIsaac G F, David M B, Gertner G Z and Goolsby D A 2001 Nitrate flux in the Mississippi River *Nature* **414** 166–7
- Milly P C D, Malyshev S L, Shevliakova E, Dunne K A, Findell K L, Gleeson T, Liang Z, Philipps P, Stouffer R J and Swenson S 2014 An enhanced model of land water and energy for global hydrologic and earth-system studies *J. Hydrometeorol.* **15** 1739–61
- Morecroft M D, Burt T P, Taylor M E and Rowland A P 2000 Effects of the 1995–1997 drought on nitrate leaching in lowland England *Soil Use Manage.* **16** 117–23
- Ogle K, Barber J J, Barron-Gafford G A, Bentley L P, Young J M, Huxman T E, Loik M E and Tissue D T 2015 Quantifying ecological memory in plant and ecosystem processes *Ecol. Lett.* **18** 221–35
- Paerl H W, Pinckney J L, Fear J M and Peierls B L 1998 Ecosystem responses to internal and watershed organic matter loading: consequences for hypoxia in the eutrophying Neuse River Estuary, North Carolina, USA *Mar. Ecol. Prog. Ser.* **166** 17–25
- Reichmann L G, Sala O E and Peters D P C 2013 Precipitation legacies in desert grassland primary production occur through previous-year tiller density *Ecology* **94** 435–43
- Sala O E, Gherardi L A, Reichmann L, Jobbagy E and Peters D 2012 Legacies of precipitation fluctuations on primary production: theory and data synthesis *Phil. Trans. R. Soc. B* **367** 3135–44
- Sheffield J, Goteti G and Wood E F 2006 Development of a 50-year high resolution global dataset of meteorological forcings for land surface modeling *J. Clim.* **19** 3088–111
- Shevliakova E, Pacala S W, Malyshev S, Hurt G C, Milly P C D, Caspersen J P, Sentman L T, Fisk J P, Wirth C and Crevoisier C 2009 Carbon cycling under 300 years of land use changes: importance of the secondary vegetation sink *Glob. Biogeochem. Cycles* **23** GB2022
- Shim J H, Pendall E, Morgan J A and Ojima D S 2009 Wetting and drying cycles drive variations in the stable carbon isotope ratio of respired carbon dioxide in semi-arid grassland *Oecologia* **160** 321–33
- Siebert S *et al* 2015 A global data set of the extent of irrigated land from 1900 to 2005 *Hydrol. Earth Syst. Sci.* **19** 1521–45

- Sinha E, Michalak A M and Balaji V 2017 Eutrophication will increase during the 21st century as a result of precipitation changes *Science* **357** 405–8
- Smith V H 2003 Eutrophication of freshwater and marine ecosystems: a global problem *Environ. Sci. Pollut. Res.* **10** 126–39
- Turner R E, Rabalais N N and Justic D 2008 Gulf of Mexico hypoxia: alternate states and a legacy *Environ. Sci. Technol.* **42** 2323–7
- UNEP 2006 Marine and coastal ecosystems and human wellbeing: a synthesis report based on the findings of the millennium ecosystem assessment (available at: www.millenniumassessment.org/en/Articlee27e.html?id=76)
- USEPA 2010 Chesapeake Bay phase 5.3 community watershed model, EPA 903S10002—CBP/TRS-303-10 (available at: <http://ches.communitymodeling.org/models/CBPhase5/documentation.php#p5modeldoc>)
- Van Beusekom J E E 2018 *Handbook on Marine Environment Protection* (Cham: Springer Nature)
- Van Drecht G, Bouwman A F, Harrison J and Knoop J M 2009 Global nitrogen and phosphate in urban wastewater for the period 1970–2050 *Glob. Biogeochem. Cycles* **23** GB0A03
- Van Meter K J, Van Cappellen P and Basu N B 2018 Legacy nitrogen may prevent achievement of water quality goals in the Gulf of Mexico *Science* **360** 427–30
- Vargas R *et al* 2011 On the multi-temporal correlation between photosynthesis and soil CO₂ efflux: reconciling lags and observations *New Phytol.* **191** 1006–17
- Vero S E, Basu N B, Van Meter K, Richards K G, Mellander P-E, Healy M G and Fenton O 2018 Review: the environmental status and implications of the nitrate time lag in Europe and North America *Hydrogeol. J.* **26** 7–22
- Wang M, Hu C, Barnes B B, Mitchum G, Lapointe B and Montoya J P 2019 The great Atlantic Sargassum belt *Science* **365** 83–87
- Ward M H, Dekok T M, Levallois P, Brender J, Gulis G, Nolan B T and Vanderslice J 2005 Workgroup report: drinking-water nitrate and health—recent findings and research needs *Environ. Health Perspect.* **113** 1607–14
- Xiang S, Doyle A, Holden P A and Schimel J P 2008 Drying and rewetting effects on C and N mineralization and microbial activity in surface and subsurface California grassland soils *Soil Biol. Biochem.* **40** 2281–9